Toward a resolvent-based statistical jet-noise model

By A. Towne, G. A. Brès† and S. K. Lele

1. Introduction

Numerous studies have identified large-scale coherent structures within turbulent jets as an important source of noise (Jordan & Colonius 2013). The spatiotemporal signatures of these structures take the form of advecting wavepackets with slowly varying wavelength and phase-speed. Although these structures make up a modest portion of the total flow energy, their spatiotemporal coherence makes them acoustically efficient compared to incoherent turbulent fluctuations. Specifically, wavepackets are correlated with the dominant aft-angle acoustic radiation. This suggests that reasonable reduced-order jet-noise models could be constructed by modeling these wavepackets.

The typical approach to modeling wavepackets is to approximate them as linear modal solutions of the Navier-Stokes equations linearized about the long-time mean of the turbulent flow field. This approach dates back to the 1970s, when it was found that certain properties of wavepackets in jets could be explained by locally parallel and weakly nonparallel linear stability theory (Mattingly & Chang 1974; Crighton & Gaster 1976). More recently, modal solutions have been obtained directly by solving parabolized stability equations (Gudmundsson & Colonius 2011; Sinha *et al.* 2014), a global eigenvalue problem (Nichols & Lele 2011; Schmidt *et al.* 2016), or a boundary value problem with specified inlet perturbations (Mohseni *et al.* 2002; Baqui *et al.* 2013; Towne & Colonius 2015).

The near-field wavepackets obtained from these linear models show compelling agreement with those educed from experimental and simulation data (Gudmundsson & Colonius 2011; Sinha *et al.* 2014). For supersonic jets, these linear solutions also contain, with reasonable accuracy, the corresponding far-field acoustic radiation (Sinha *et al.* 2014). On the other hand, linear models for subsonic jets underpredict far-field acoustic radiation by as much as 40 dB despite the close match in the near-field wavepacket (Baqui *et al.* 2013; Jordan *et al.* 2014).

A hypothesized explanation for this discrepancy is acoustic amplification due to wave-packet intermittency, or jitter (Cavalieri *et al.* 2011). Unlike the wavepackets obtained from linear models, real wavepackets in turbulent jets undergo intermittent, low-frequency modulation of their envelope and phase. The acoustic efficiency of a wavepacket is highly sensitive to these modulations, so flow events that lead to small near-field changes in the wavepacket can give rise to large amplifications in the acoustic field. This suggests that the average wavepacket does not produce the average sound, a conclusion also reached via statistical analysis of simulation data from both low-Reynolds-number and high-Reynolds-number subsonic jets (Freund & Colonius 2009; Towne *et al.* 2015). In other words, noise production is sensitive to second-order flow statistics that are not properly captured by linear models (Cavalieri & Agarwal 2014).

† Cascade Technologies, Inc.

This has led to renewed interest in wavepacket models that account, in one way or another, for nonlinear effects within the turbulent flow. These models can be sorted into two broad categories: those that explicitly retain some small subset of the nonlinear interactions among large-scale coherent structures and those that model the nonlinear terms as an external forcing on the linear dynamics.

A number of variations exist within the first category. Several authors (Malik & Chang 2000; Cheung & Lele 2007; Itasse *et al.* 2015) have used the nonlinear parabolized stability equations, which in an approximate sense account for nonlinear interactions between the dominant weakly nonparallel instability modes at a discrete set of frequencies and azimuthal wavenumbers. Sandham *et al.* (2006) and Suponitsky *et al.* (2010) developed models that focus on low-frequency difference modes resulting from the nonlinear interaction between two instability waves with similar frequencies. Similarly, Wu & Huerre (2009) derived an asymptotic model that describes low-frequency acoustic radiation resulting from the nonlinear interaction between a pair of helical instability modes with nearly the same frequencies but opposite azimuthal wavenumbers. All three of the preceding approaches have been validated primarily in low-Reynolds-number transitional jets or in jets that undergo harmonic actuation at (or upstream of) the nozzle exit. Whether these mechanisms are also relevant in realistic high-Reynolds-number turbulent jets has not been established.

Also fitting within this first category is the work of Jordan *et al.* (2014), who studied the effect of a slowly varying mean flow on the intermittency and acoustic efficiency of wavepackets in a subsonic turbulent jet. This amounts to retaining nonlinear interactions between wavepackets and low-frequency fluctuations. They found that accounting for intermittency in this way increased the acoustic output of the wavepackets by up to 20 dB at peak aft angles, but there remained a discrepancy of as much as 20 dB compared to the experimental acoustic field.

The second category includes a number of stochastic models. Bechara *et al.* (1994) introduced the stochastic noise generation and radiation model, in which the forcing is defined by a random time-dependent velocity field whose statistical properties mimic homogeneous isotropic turbulence. The model was modified by Billson *et al.* (2004) and Lafitte *et al.* (2011) to account for anisotropy and turbulent sweeping effects, respectively. Siefert & Ewert (2009) developed a similar approach in which stochastic velocities with prescribed statistics are generated using the random particle-mesh method and used to realize the source terms suggested by Tam & Auriault (1999).

A somewhat different approach that fits within the second category is resolvent analysis, which has it roots in linear-systems theory and has been applied to jets by Garnaud *et al.* (2013), Jeun *et al.* (2016), and Semeraro *et al.* (2016). In this approach, the Navier-Stokes equations are modeled as a linear input/output system in which the nonlinear terms are the input and any linear combinations of the flow variables is the output. The frequency-space transfer function between the input and output is called the resolvent operator and is related to the linearized Navier-Stokes operator. The leading singular modes (computed via singular value decomposition) maximize the gain, which is given by the corresponding singular value, between the input and output.

The two broadly defined categories discussed above make very different assumptions regarding the nature and role of the nonlinear effects that are most important for jet-noise production. To address this, Towne *et al.* (2015) and Towne (2016) used the large-eddy simulation (LES) database of Brès *et al.* (2015, 2016) to directly compute the nonlinear forcing terms for a Mach 0.9 turbulent jet and analyzed the flow and forcing data using

empirical modal-decomposition techniques. Modes with high energy were extracted using proper orthogonal decomposition, while high-gain modes were identified using a novel technique called empirical resolvent-mode decomposition. In contrast to the flow and acoustic fields, the forcing field is characterized by a lack of energetic coherent structures. Furthermore, the structures that do exist are largely uncorrelated with the acoustic field. Instead, the forcings that most efficiently excite an acoustic response appear to take the form of random turbulent fluctuations that jitter the wavepackets, implying that direct feedback from nonlinear interactions among wavepackets is not an essential noise source mechanism in high-Reynolds-number jets. This suggests that the essential ingredients of sound generation are contained within the linearized Navier-Stokes operator rather than in the nonlinear terms. Overall, these results support the validity of jet-noise models that treat nonlinearity as an external excitation.

With this motivation, this paper lays the groundwork for an improved resolvent-based approach to jet-noise modeling centered on a statistical description of the stochastic dynamics of the jet. We begin in Section 2 by showing that the resolvent framework can be used to relate second-order statistics of the flow variables and the nonlinear forcing terms. This relationship shows that resolvent modes provide an optimal representation of the flow only if the nonlinear forcing terms consist of unit-amplitude white-noise, but also provide a foundation for systematically accounting for correlated forcing. In Section 3, we use LES data to study the statistics of the true nonlinear forcing terms in a high-Reynolds-number jet with the goal of gaining insight into how they should be approximated within a resolvent-based model. Finally, we summarize the main results and discuss some ongoing aspects of the project in Section 4.

2. A statistical perspective on resolvent analysis

The dynamics of turbulent jets are stochastic due to the sensitivity of the flow to random external excitations. In experiments, these excitations consist of incoming turbulence from the nozzle, environmental fluctuations, acoustic reflections within the experimental facility, and so on. In simulations, examples include synthetic turbulence that is injected in the nozzle to mimic experimental conditions and numerical round-off errors. Because of this inherent randomness, the properties of the flow are best described by statistical quantities defined in terms of the expectation operator. In this section, we will show how the resolvent framework, which is usually understood in terms of periodic (deterministic) signals, can be used to relate second-order statistics of the flow variables and the nonlinear forcing terms.

We begin with the full compressible Navier-Stokes equations, which can be written conceptually as

$$\frac{\partial q}{\partial t} = \mathcal{F}(q), \tag{2.1}$$

where q is a state-vector of flow variables. Substituting the standard Reynolds decomposition

$$q(x, r, \theta, t) = \bar{q}(x, r) + q'(x, r, \theta, t) \tag{2.2}$$

into Eq. (2.1) and isolating the terms that are linear in q' yields an equation of the form

$$\frac{\partial q'}{\partial t} - \mathcal{A}(\bar{q}) q' = f(\bar{q}, q'), \tag{2.3}$$

where

$$\mathcal{A}(\bar{q}) = \frac{\partial \mathcal{F}}{\partial q}(\bar{q}) \tag{2.4}$$

and f contains the remaining nonlinear terms. It is usually the case that only a limited portion of the state q' is of interest. This can be formalized by defining an output quantity,

$$y = \mathcal{C}q', \tag{2.5}$$

consisting of any linear combination of the state. For example, y could represent the far-field acoustic pressure.

Since the jet is round and statistically stationary, it is valid to apply Fourier transforms in the azimuthal direction and time to Eqs. (2.3) and (2.5), giving

$$(i\omega I - \mathcal{A}_m)\hat{q} = \hat{f}, \tag{2.6}$$

$$\hat{y} = \mathcal{C}\hat{q}, \tag{2.7}$$

where ω is the angular frequency, m is the azimuthal wavenumber, and $\mathcal{A}_m$ is the operator $\mathcal{A}$ with $\frac{\partial}{\partial \theta}$ replaced by im. The transformed variables $\hat{q}$, $\hat{y}$, $\hat{f}$ are functions of (x, r, m, ω). The input/output relation between the nonlinear (input) term $\hat{f}$ and the output $\hat{y}$ is obtained by eliminating $\hat{q}$ from Eqs. (2.6)-(2.7), giving

$$\hat{y} = \mathcal{R}\hat{f}, \tag{2.8}$$

with

$$\mathcal{R} = \mathcal{C}(i\omega I - \mathcal{A}_m)^{-1}. \tag{2.9}$$

Note that $(i\omega I - \mathcal{A}_m)$ is always invertible if $\mathcal{A}$ is stable; i.e., the real part of all of its eigenvalues is negative.

Resolvent modes are given by the singular value decomposition of the resolvent operator,

$$\mathcal{R} = U\Sigma V^*. \tag{2.10}$$

The singular values, which appear within the diagonal positive-semidefinite matrix Σ, give the square root of the optimal gains between the input and output modes defined by the right and left singular vectors contained in the columns of the orthonormal matrices V and U, respectively. The asterisk indicates a conjugate transpose.

The second-order statistics of the input and output are obtained by averaging over an ensemble of solutions of Eq. (2.1) that have undergone different random external excitation. Specifically, we define the cross-spectral-density (CSD) matrices $S_{\hat{y}\hat{y}} = \langle \hat{y}\hat{y}^* \rangle$ and $S_{\hat{f}\hat{f}} = \langle \hat{f}\hat{f}^* \rangle$, where $\langle \cdot \rangle$ is the expectation operator. Using Eq. (2.8), these two CSD matrices are related as

$$S_{\hat{y}\hat{y}} = \langle \hat{y}\hat{y}^* \rangle = \langle \mathcal{R}\hat{f}\hat{f}^*\mathcal{R}^* \rangle = \mathcal{R}\langle \hat{f}\hat{f}^* \rangle \mathcal{R}^* = \mathcal{R}S_{\hat{f}\hat{f}}\mathcal{R}^*. \tag{2.11}$$

Equation (2.6) provides an exact relationship between the second-order statistics of the nonlinear term $\hat{f}$ and the output $\hat{y}$ in terms of the resolvent operator $\mathcal{R}$.

If the nonlinear forcing term is completely uncorrelated in space and time with equal amplitude everywhere is space, then its CSD matrix is the identity, $S_{\hat{f}\hat{f}} = I$. Such a forcing corresponds to unit-amplitude white-noise. In this case, the CSD of the output is completely defined by the resolvent operator, and Eq. (2.11) becomes

$$S_{\hat{y}\hat{y}} = \mathcal{R}\mathcal{R}^* = U\Sigma V^*V\Sigma U^* = U\Sigma^2 U^*. \tag{2.12}$$

Since U is orthonormal, the last expression in Eq. (2.12) shows that the resolvent output modes are the principal components of the output CSD matrix, i.e., the proper-orthogonal-decomposition (POD) modes of $\hat{q}$, if the forcing is unit-amplitude white-noise. This result was recently independently derived by Semeraro *et al.* (2016).

Equations (2.11) and (2.12) show that standard resolvent modes provide an optimal representation of the output only if the nonlinear forcing term consists of unit-amplitude white-noise. However, Eq. (2.11) also provides the foundation for systematically incorporating correlated nonlinear forcing into the resolvent framework. To do so, we begin with a factorization of the forcing CSD of the form

$$S_{\hat{f}\hat{f}} = FF^*, \tag{2.13}$$

which can represent a Cholesky decomposition or a POD eigenvalue decomposition $S_{\hat{f}\hat{f}} = V_F \Sigma_F^2 V_F^*$ with $F = V_F \Sigma_F$. Next, we define a modified resolvent operator

$$\tilde{\mathcal{R}} = \mathcal{R}F \tag{2.14}$$

and its singular value decomposition

$$\tilde{\mathcal{R}} = \tilde{U}\tilde{\Sigma}\tilde{V}^*. \tag{2.15}$$

Unless F is orthonormal (which is the case when the forcing is white), the singular values and vectors of $\mathcal{R}$ and $\tilde{\mathcal{R}}$ are not the same; including the correlated forcing fundamentally alters the modes. Eq. (2.11) can be written in terms of the modified resolvent operator as

$$S_{\hat{y}\hat{y}} = \tilde{\mathcal{R}}\tilde{\mathcal{R}}^* = \tilde{U}\tilde{\Sigma}\tilde{V}^*\tilde{V}\tilde{\Sigma}\tilde{U}^* = \tilde{U}\tilde{\Sigma}^2\tilde{U}^*. \tag{2.16}$$

Therefore, the output modes of the modified resolvent operator are the POD modes of $\hat{y}$. Furthermore, the gains give the energy in each mode. As a result, the modified resolvent modes provide an optimal representation of the output. The remaining task in obtaining a predictive model is to construct an appropriate approximation of the forcing CSD matrix $S_{\hat{f}\hat{f}}$.

3. Analysis of the nonlinear forcing terms in a Mach 0.9 jet

In this section, we use LES data of a Mach 0.9 turbulent jet to study the form of the CSD matrix $S_{\hat{f}\hat{f}}$ with the goals of evaluating the unit-amplitude white-noise assumption that is implicit within the standard resolvent approach and obtaining guidance for modeling $S_{\hat{f}\hat{f}}$.

3.1. *LES database and spectral estimation*

We use data from a high-fidelity large eddy simulation (LES) of an isothermal Mach 0.9 jet issued from a convergent-straight nozzle. The simulation was performed with the compressible flow solver CharLES developed at Cascade Technologies (Brès *et al.* 2016). The Reynolds number based on the nozzle diameter is one million and the boundary layer is fully turbulent at the nozzle exit. The accuracy of the LES data was verified via extensive comparison with experimental measurements. More information on the LES and validation are available in Brès *et al.* (2015, 2016). The nonlinear forcing terms are computed using the LES code. This ensures consistency with the LES approximation of the Navier-Stokes equations and minimizes numerical contamination compared to alternative methods. Additional details can be found in Towne (2016).

Spectra are estimated using Welch's method. The flow and forcing time series are
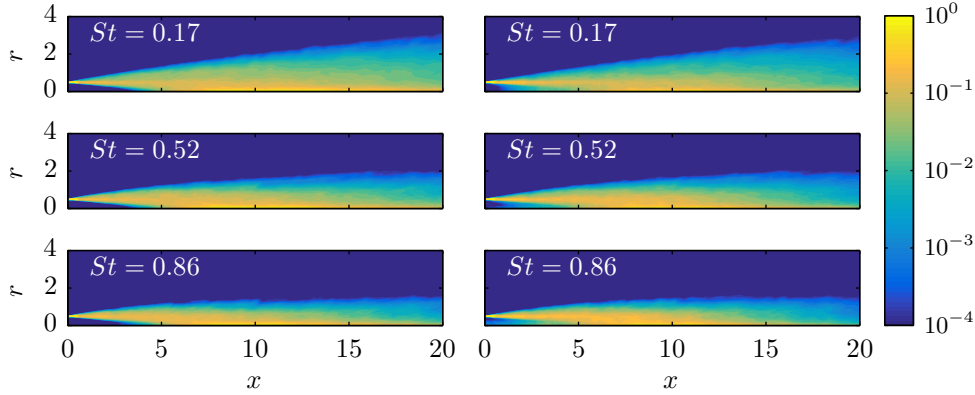
FIGURE 1. Power spectral densities of the streamwise-momentum forcing (left column) and energy forcing (right column) at $St = 0.17$, 0.52, and 0.86 and $m = 0$.

partitioned into an ensemble of overlapping blocks, windowed, and transformed in time and azimuth using a discrete Fourier transform. We use blocks containing 256 instantaneous snapshots (covering about 50 acoustic time units) with 90% overlap and a standard Hann window. We have verified that our conclusions are not sensitive to these choices. The cross-spectra of the resulting Fourier modes are then ensemble-averaged to obtain the CSD matrix for each frequency–azimuthal wavenumber pair. Precisely,

$$S_{\hat{u}\hat{v}}\left(\vec{x}_i, \vec{x}_j, m, \omega\right) = \frac{1}{N} \sum_{k=1}^{N} \hat{u}^{(k)}\left(\vec{x}_i, m, \omega\right) \left(\hat{v}^{(k)}\left(\vec{x}_j, m, \omega\right)\right)^*, \qquad (3.1)$$

where $N = 356$ is the number of blocks, $\vec{x} = (x, r)$, and $\hat{u}^{(k)}$ and $\hat{v}^{(k)}$ are the Fourier modes of any two components of the input or output in the k-th block.

3.2. *Power spectral densities*

We begin by focusing on the power spectral densities (PSDs) $S_{\hat{u}\hat{u}}\left(\vec{x}_i, \vec{x}_i, m, \omega\right)$, which make up the diagonal entries in the CSD matrices. The PSDs of the asymmetric $(m = 0)$ portion of the streamwise-momentum and energy forcing terms for three frequencies are shown in Figure 1. These results are characteristic of those observed for all five components of the nonlinear forcing term and for all intermediate frequencies. The frequencies are reported in terms of the Strouhal number $St = fD/U_j$, where D is the diameter of the nozzle exit, U_j is the jet velocity at the nozzle exit, and $f = \omega/2\pi$. The contour levels are logarithmically spaced and span four orders-of-magnitude (smaller values are saturated at the minimum level). No frequency-dependent scaling has been applied, but a single fixed (frequency-independent) parameter was used to scale the magnitude of the energy-equation forcing terms to the same level as the streamwise-momentum forcing terms.

The PSDs of both the streamwise-momentum and energy components of the forcing (as well as the other three components that are not shown) exhibit a remarkable degree of frequency independence. This is not a visual artifact of the logarithmically distributed contour levels; the relative difference between the spatially averaged PSD at different frequencies is less than 6% for all five components of the forcing within the range $0.1 < St < 1$ (and below 1% in all but a few cases). Therefore, within this frequency range (and for $m = 0$), the nonlinear forcing is nearly white-in-time. However, all components of
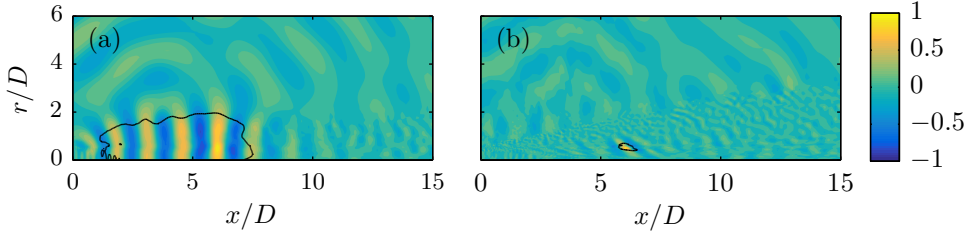
FIGURE 2. The real part of the complex coherence of (a) pressure and (b) streamwise-momentum forcing with respect to their reference values at $x_0/D = 6, r_0/D = 0.5$ for $St = 0.52$ and $m = 0$. The black lines bound the regions where the magnitude of the coherence is greater than 0.5.

the PSD have a clear and consistent spatial structure. The forcing is essentially confined within the slowly spreading shear-layer up to the end of the potential core and within the turbulent near-field of the fully-developed jet farther downstream. The magnitude of the forcing away from the jet and within the potential core is nearly zero. The only differences observed between the different frequencies occur well downstream along the outer fringes of the jet, a region that is not expected to be important for sound generation. Finally, as mentioned already, the amplitude of the forcing is different for different components of the nonlinear forcing (but the same for every frequency). Specifically, the three momentum forcing terms have nearly equal amplitude, whereas the mass and energy forcing terms are less energetic by nearly two orders-of-magnitude. In contrast to these results, the PSDs of each flow variable have different spatial distributions that are strongly dependent on frequency.

3.3. *Cross-spectral densities*

The remaining off-diagonal terms in the CSD matrices are made up of correlations between every combination of variable and spatial coordinates. The magnitude of each entry depends strongly on the PSDs of the two involved terms ($\hat{u}$ and $\hat{v}$), so it is convenient to instead work with the scaled quantity

$$\gamma_{\hat{u}\hat{v}}(\vec{x}_i, \vec{x}_j, m, \omega) = \frac{S_{\hat{u}\hat{v}}(\vec{x}_i, \vec{x}_j, m, \omega)}{\sqrt{S_{\hat{u}\hat{u}}(\vec{x}_i, \vec{x}_i, m, \omega)}\sqrt{S_{\hat{v}\hat{v}}(\vec{x}_j, \vec{x}_j, m, \omega)}}. \tag{3.2}$$

We call $\gamma_{\hat{u}\hat{v}}$ the complex coherence, and the standard definition of coherence is given by its magnitude $|\gamma_{\hat{u}\hat{v}}|$. By construction, the coherence satisfies the condition $0 \leq |\gamma_{\hat{u}\hat{v}}| \leq 1$. Large and small values indicate strong and weak relationships, respectively, between $\hat{u}$ and $\hat{v}$.

The wavepackets within the jet cause extended regions of high coherence within the flow variables. For example, the contours in Figure 2(a) show the real part of the complex coherence of the pressure field, relative to the pressure at the reference point $(x_0/D = 5, r_0/D = 0.5)$ for $St = 0.52$ and $m = 0$. The wavepacket structure is evident, and the region where the magnitude of the coherence is greater than one-half (demarcated by the solid line) extends more than six jet diameters in the streamwise direction and two jet diameters in the radial direction. Figure 3 shows streamwise (top row) and radial (bottom row) slices of the coherence of the pressure field relative to the pressure at three different reference points (columns) for $St = 0.17, 0.52$, and 0.86 and $m = 0$. The streamwise wavelength and decay rate and the radial form of the wavepackets in the coherence field depend strongly on frequency and the location of the reference point, as previously observed by Jaunet *et al.* (2016). These variations can be attributed, at least
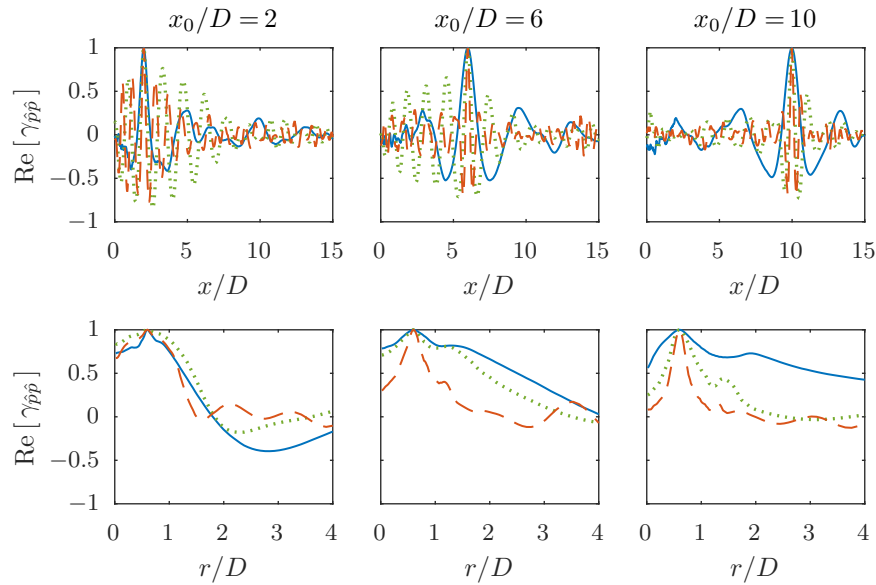
FIGURE 3. The real part of the complex coherence of the pressure with respect to its reference values at $r_0/D = 0.5$ and $x_0/D = 2$, 6, and 10 (left to right), plotted along the lines $r/D = 0.5$ (top row) and $x/D = x_0/D$ (bottom row) for $m = 0$ and (———) $St = 0.17$; (------) $St = 0.52$; (— — —) $St = 0.86$.

in part, to the frequency and streamwise dependence of the Kelvin-Helmholtz modes whose growth and decay play a central role in the formation of wavepackets.

In contrast, the coherence of the nonlinear forcing fields is highly localized and nearly frequency independent. The contours in Figure 2(b) show the real part of the complex coherence of the streamwise-momentum forcing, relative to the streamwise-momentum forcing at $(x_0/D = 5, r_0/D = 0.5)$ for $St = 0.52$ and $m = 0$. The streamwise and radial extent of the region where the coherence is larger than one-half is about an order-of-magnitude smaller than it was for the pressure. The coherent region is slightly inclined and elongated in the streamwise direction. Figure 4 shows streamwise and radial slices of the correlation of the streamwise-momentum forcing field relative to its value for the same three reference points and frequencies as before. In all cases, the coherence consists of a narrow spike at the reference point surrounded by low-level noise (the amplitude of which is related to the convergence of the data). The shape and width of the spike are nearly independent of frequency. The peak is extremely narrow in the initial shear layer and broadens as the reference point is moved downstream. There is some evidence of a frequency-dependent streamwise wavenumber, but the frequency-independent decay rate is so large that this seems to constitute a secondary effect.

The CSD matrices also contain intervariable correlations (between pressure and velocity, for example). Figure 5 shows the coherence along $r/D = 0.5$ of the streamwise-velocity field relative to the pressure (top row) and of the energy forcing field relative to the streamwise-momentum forcing field for the same three reference points and frequencies. The velocity/pressure coherence reaches significant levels and again exhibits a clear wavepacket structure. On the other hand, the energy/momentum forcing coherence appears to be negligible, although it is possible that the statistical noise floor of the data might be obscuring low-amplitude peaks.
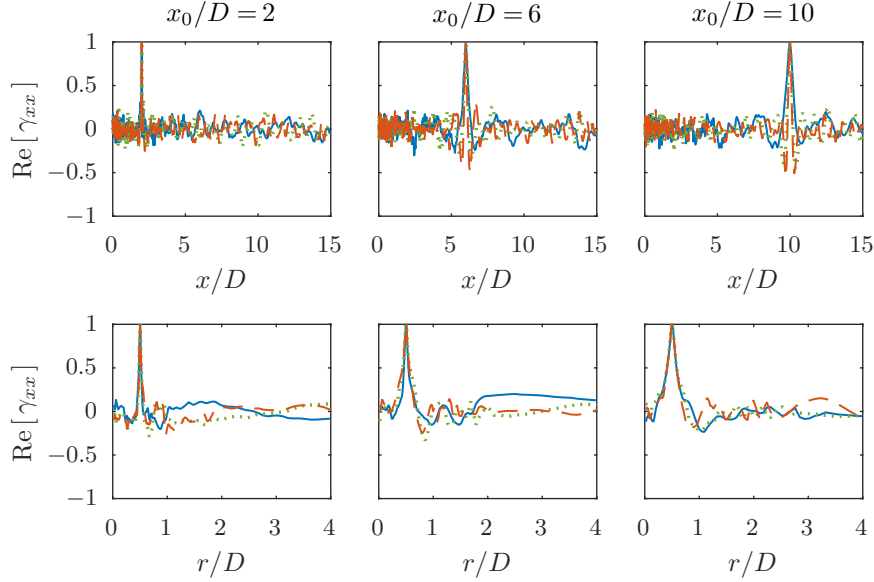
FIGURE 4. The real part of the complex coherence of the streamwise-momentum forcing with respect to its reference values at $r_0/D = 0.5$ and $x_0/D = 2$, 6, and 10 (left to right), plotted along the lines $r/D = 0.5$ (top row) and $x/D = x_0/D$ (bottom row) for $m = 0$ and (———) $St = 0.17$; (-------) $St = 0.52$; (— — —) $St = 0.86$.

3.4. *Implications for modeling*

We now explicitly compare the results from the last two subsections to the unit-amplitude white-noise approximation $S_{\hat{f}\hat{f}} = I$ that is implicit in standard resolvent models.

First, $S_{\hat{f}\hat{f}} = I$ implies that the forcing is white-in-time. Since both the CSD and coherence of the nonlinear forcing term are mostly frequency independent, this proves to be a valid approximation.

Second, $S_{\hat{f}\hat{f}} = I$ implies that the PSD of the forcing is equal for all components and for all spatial locations. In reality, the PSD is larger for the three momentum components of the forcing than for the mass and energy components and (for all components) varies by many orders-of-magnitude as a function of spatial location. Of particular relevance is the observation that the PSD is nearly zero in the potential core. The leading input modes obtained by previous investigators have significant amplitude (and in some cases even peak) within this region. As a result, properly accounting for the spatial distribution of the forcing PSD will likely significantly alter the leading output resolvent modes.

Third, $S_{\hat{f}\hat{f}} = I$ implies zero coherence between any two distinct points; i.e., the coherence consists of a Dirac delta function at the reference point location. The coherence of the forcing data showed narrow peaks whose width depends on the location of the reference point. Since the peaks are quite narrow up to the end of the potential core, it is unclear whether accounting for their non-zero width will have a meaningful impact on the modified resolvent modes.

Fourth, $S_{\hat{f}\hat{f}} = I$ implies zero coherence between different components of the forcing, even at the same location. This appears to be a reasonable approximation in the isothermal jet considered here, but these terms could become important in heated jets.
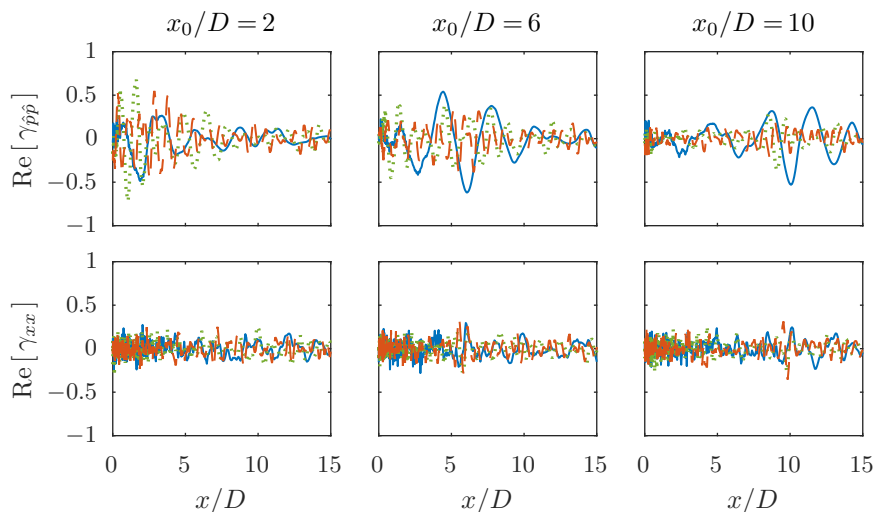
FIGURE 5. The real part of the complex coherence of the streamwise-velocity with respect to the pressure (top row) and of the energy forcing with respect to the streamwise-momentum forcing (bottom row) with the reference points $r_0/D = 0.5$ and $x_0/D = 2$, 6, and 10 (left to right), plotted along the line $r/D = 0.5$ for $m = 0$ and (———) $St = 0.17$; (------) $St = 0.52$; (− − −) $St = 0.86$.
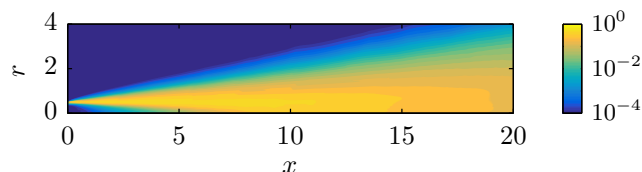

FIGURE 6. Turbulent kinetic energy computed from the LES data, scaled by its maximum value and plotted using the same logarithmic scale used in Figure 1.

4. Conclusions and future work

This paper lays the groundwork for improved resolvent-based models that account for the statistics of the nonlinear forcing terms. By deriving an expression that relates the second-order statistics of the flow variables and the nonlinear forcing term, we showed that the leading modes of the standard resolvent operator provide an optimal representation of the jet only if the nonlinear forcing terms are unit-amplitude white-noise. Then, we used LES data to study the statistics of the true nonlinear forcing terms in a high-Reynolds-number subsonic jet.

Overall, while the unit-amplitude white-noise approximation is shown to be reasonable in some regards, it is also apparent that there is significant room for improvement, especially with respect to the spatial distribution of forcing energy. Furthermore, the near frequency independence of the forcing PSD and coherence makes these quantities amenable to modeling. In an ongoing effort, we are seeking a model for these quantities whose parameters depend solely on quantities that can be extracted from a Reynolds-averaged Navier-Stokes (RANS) simulation. In particular, we have found that the forcing PSD can be reasonably modeled by the turbulent kinetic energy, which is plotted in Figure 6 using the same logarithmic scale used in Figure 1. Additionally, spatially dependent length scales that could be used to model the coherence peaks can be obtained from basic

RANS turbulence models. The final goal of this work is to obtain a predictive, quantitatively accurate, reduced-order jet-noise model.

Acknowledgments

REFERENCES

BAQUI, Y. B., AGARWAL, A., CAVALIERI, A. & SINAYOKO, S. 2013 Nonlinear and linear noise source mechanisms in subsonic jets. *AIAA Paper* 2013-2279.

BECHARA, W., BAILLY, C., LAFON, P. & CANDEL, S. M. 1994 Stochastic approach to noise modeling for free turbulent flows. *AIAA J.* **32**, 455–463.

BILLSON, M., ERIKSSON, L.-E. & DAVIDSON, L. 2004 Jet noise modeling using synthetic anisotropic turbulence. *AIAA Paper* 2004-3028.

BRÈS, G. A., HAM, F. E., NICHOLS, J. W., JORDAN, P. & LELE, S. K. 2016 Unstructured large eddy simulations of supersonic jets. *AIAA J.* (In Press).

BRÈS, G. A., JAUNET, J., LE RALLIC, M., JORDAN, P., COLONIUS, T. & LELE, S. K. 2015 Large eddy simulation for jet noise: the importance of getting the boundary layer right. *AIAA Paper* 2015-2535.

BRÈS, G. A., JAUNET, V., LE RALLIC, M., JORDAN, P., TOWNE, A., SCHMIDT, O., COLONIUS, T., CAVALIERI, A. V. G. & LELE, S. K. 2016 Large eddy simulation for jet noise: azimuthal decomposition and intermittency of the radiated sound. *AIAA Paper* 2016-3050.

CAVALIERI, A. V. G. & AGARWAL, A. 2014 Coherence decay and its impact on sound radiation by wavepackets. *J. Fluid Mech.* **748**, 399–415.

CAVALIERI, A. V. G., JORDAN, P., AGARWAL, A. & GERVAIS, Y. 2011 Jittering wavepacket models for subsonic jet noise. *J. Sound Vib.* **330**, 4474–4492.

CHEUNG, L. & LELE, S. 2007 *Aeroacoustic noise prediction and the dynamics of shear layers and jets using the nonlinear parabolized stability equations.* Tech. Rep. No. TF-103, Stanford University.

CRIGHTON, D. G. & GASTER, M. 1976 Stability of slowly diverging jet flow. *J. Fluid Mech.* **77**, 397–413.

FREUND, J. & COLONIUS, T. 2009 Turbulence and sound-field POD analysis of a turbulent jet. *Int. J. Aeroacoust.* **8**, 337–354.

GARNAUD, X., LESSHAFFT, L., SCHMID, P. & HUERRE, P. 2013 The preferred mode of incompressible jets: linear frequency response analysis. *J. Fluid Mech.* **716**, 189–202.

GUDMUNDSSON, K. & COLONIUS, T. 2011 Instability wave models for the near-field fluctuations of turbulent jets. *J. Fluid Mech.* **689**, 97–128.

ITASSE, M., BRAZIER, J.-P., LÉON, O. & CASALIS, G. 2015 Parabolized stability equations analysis of nonlinear interactions with forced eigenmodes to control subsonic jet instabilities. *Phys. Fluids* **27**, 084106.

JAUNET, V., JORDAN, P. & CAVALIERI, A. V. G. 2016 Two-point coherence of wavepackets in turbulent jets. *AIAA Paper* 2016-3058.

JEUN, J., NICHOLS, J. W. & JOVANOVIĆ, M. R. 2016 Input-output analysis of high-speed axisymmetric isothermal jet noise. *Phys. Fluids* **28**, 047101.

JORDAN, P. & COLONIUS, T. 2013 Wave packets and turbulent jet noise. *Annu. Rev. Fluid Mech.* **45**, 173–195.

JORDAN, P., COLONIUS, T., BRÈS, G. A., ZHANG, M., TOWNE, A. & LELE, S. 2014 Modeling intermittent wavepackets and their radiated sound in a turbulent jet. *Proceedings of the Summer Program*, Center for Turbulence Research, Stanford University, pp. 241–249.

LAFITTE, A., LAURENDEAU, E., LA GARREC, T. & BAILLY, C. 2011 A study based on the sweeping hypothesis to generate stochastic turbulence. *AIAA Paper* 2011-2888.

MALIK, M. & CHANG, C.-L. 2000 Nonparallel and nonlinear stability of supersonic jet flow. *Comput. Fluids.* **29**, 327–365.

MATTINGLY, G. E. & CHANG, C. C. 1974 Unstable waves on an axisymmetric jet column. *J. Fluid Mech.* **65**, 541–560.

MOHSENI, K., COLONIUS, T. & FREUND, J. B. 2002 An evaluation of linear instability waves as sources of sound in a supersonic turbulent jet. *Phys. Fluids* **14**, 3593–3600.

NICHOLS, J. & LELE, S. 2011 Global modes and transient response of a cold supersonic jet. *J. Fluid Mech.* **669**, 225–241.

SANDHAM, N. D., MORFEY, C. & HU, Z. 2006 Nonlinear mechanisms of sound generation in a perturbed parallel jet flow. *J. Fluid Mech.* **565**, 1–23.

SCHMIDT, O. T., TOWNE, A., COLONIUS, T., JORDAN, P., JAUNET, V., CAVALIERI, A. V. G., & BRÈS, G. A. 2016 Super- and multi-directive acoustic radiation by linear global modes of a turbulent jet. *AIAA Paper* 2016-2808.

SEMERARO, O., JAUNET, V., JORDAN, P., CAVALIERI, A. V. G. & LESSHAFFT, L. 2016 Stochastic and harmonic optimal forcing in subsonic jets. *AIAA Paper* 2016-2935.

SIEFERT, M. & EWERT, R. 2009 Sweeping sound generation in jets realized with a random particle-mesh method. *AIAA Paper* 2009-3369.

SINHA, A., RODRIGUEZ, D., BRÈS, G. A. & COLONIUS, T. 2014 Wavepacket models for supersonic jet noise. *J. Fluid Mech.* **742**, 71–95.

SUPONITSKY, V., SANDHAM, N. D. & MORFEY, C. L. 2010 Linear and nonlinear mechanisms of sound radiation by instability waves in subsonic jets. *J. Fluid Mech.* **658**, 509–538.

TAM, C. K. W. & AURIAULT, L. 1999 Jet mixing noise from fine-scale turbulence. *AIAA J.* **37**, 145–153.

TOWNE, A. 2016 *Advancements in jet turbulence and noise modeling: accurate one-way solutions and empirical evaluation of the nonlinear forcing of wavepackets.* PhD thesis, California Institute of Technology.

TOWNE, A. & COLONIUS, T. 2015 One-way spatial integration of hyperbolic equations. *J. Comput. Phys.* **300**, 844–861.

TOWNE, A., COLONIUS, T., JORDAN, P., CAVALIERI, A. V. G. & BRÈS, G. A. 2015 Stochastic and nonlinear forcing of wavepackets in a Mach 0.9 jet. *AIAA Paper* 2015-2217.

WU, X. & HUERRE, P. 2009 Low-frequency sound radiated by a nonlinearly modulated wavepacket of helical modes on a subsonic circular jet. *J. Fluid Mech.* **637**, 173–211.